NANOMATERIALS
SCIENCE & ENGINEERING
Vol. 2, No. 4, pp. 183-197 (2020)

RESEARCH ARTICLE

https://doi.org/10.34624/nmse.v2i4.22873

Modeling of the 2D-materials hybrid nanostructures based on ferroelectric polymer PVDF/P(VDF-TrFE) and MoS_2 dichalcogenide

V. S. Bystrov[1, *], E.V. Paramonova[1], A.V. Sapronova[1,2], Hong Shen[3], Xiangjian Meng[3], Jianlu Wang[3], L.A. Avakyan[4]

[1] Institute of Mathematical Problems of Biology, Keldysh Institute of Applied Mathematics, RAS, 142290 Pushchino, Moscow region, Russia
[2] PetraOS AS, Straume, 5353, Norway
[3]Shanghai Institute of Technical Physics, Chinese Academy of Sciences, Shanghai 200083, China
[4]Southern Federal University, Department of Physics, 344090 Rostov-on-Don, Russia
**Corresponding author, e-mail address: vsbys@mail.ru*

Received 3 November 2020; accepted 10 December 2020; published online 15 December 2020

ABSTRACT

Transition metal dichalcogenide MoS_2 monolayers is very promising for many applications, especially in the fields of optics as emitters and detectors, in electronics as transistors. It is first of all due that they have a direct band gap E_g, which is dependent on external applied electric fields.

To create such an electric field, it is proposed to use the field induced polarization of ferroelectric polymers such as PVDF and P(VDF-TrFE). These polymers in the ferroelectric phase are capable to create significant polarization in very thin layers, about 5 Å. By combining such ferroelectric layers and MoS_2 layers, hybrid nanostructures can be created, that are convenient for design of new photodetectors with controlled properties. The prominent properties of this hybrid structure arise and benefit namely from the ferroelectric-polarization-induced ultra-high electric field of the PVDF or P(VDF-TrFE), that impact on MoS_2 layers and control the band gap E_g.

In this work, we simulate such a hybrid structure based on PVDF and MoS_2 layers and study their features and properties. For calculating MoS_2, the methods of density functional theory (DFT) are used, implemented in the VASP program. Semi-empirical methods based on the HyperChem software package are used to model and study both individual layers of the hybrid structure and the features of their joint interaction. The results obtained convincingly show a strong influence on the width of the MoS_2 bandgap E_g from the side of the PVDF layers, creating polarization P and an electric field E, which affects MoS_2 layers. In addition, the dependence of the band gap E_g under the action of electric field E from the distance between the layers PVDF and MoS_2 has been established.

1. INTRODUCTION

Transition metal dichalcogenides (TMD) constitute an important class of 2D materials: they have great potential for future applications as photodetector components due to their excellent optoelectronic performance [1, 2]. Bulk dichalcogenide materials have been studied for several decades, however, only recently new approaches to the creation and study of nanoscale devices have opened up new possibilities for using monolayers with molybdenum disulfide (MoS_2), tungsten (WS_2), and other TMDs in nanoelectronics and optoelectronics. Layered molybdenum and tungsten dichalcogenides are semiconductors with a band gap of 1.3–2.1 eV, while bulk materials are indirect-gap semiconductors, but monolayers are direct-gap semiconductors [2, 3].

Naturally, such 2D materials have attracted much attention in the last decade for the manufacture of photodetectors [3 - 5]. Among them, the optoelectronic properties of the field-effect transistor, especially for the MoS_2 photodetector (sometimes called the phototransistor), have attracted the most intense attention of researchers.

Here, photodetectors and transistors based on, for example, 2D graphene [6, 7] and MoS_2, as well as their combinations, including those with other van der Waals structures [8], are promising.

On the other hand, the use of the properties of organic polymer ferroelectrics (FEP) [9-11], especially the discovery of two-dimensional ferroelectrics based on polymers (FEP) such as polyvinylidene fluoride (PVDF) and its copolymer with trifluoroethylene - polyvinylidene fluoride-trifluoroethylene P(VDF-TrFE) [12-22] turned out to be a significant breakthrough here, as it made it possible to create more and more efficient and at the same time nanoscale composite structures that have an ever wider range of adjustable properties, including pyroelectric, optical and piezoelectric properties) [9 - 22]. At the same time, composite nanostructures based on PVDF/ P(VDF-TrFE) in combination with Graphene/Graphene oxide [23-27]) are now being created and studied here. Note that in the study of such nanomaterials, computer methods for modeling structures and calculating the physical properties of these materials are also widely used [16-27].

As a result, interest in such new composite and hybrid nanomaterials with a two-dimensional structure (2D materials) has grown dramatically recently. Thus, in [4], it is proposed to use MoS_2 in combination with an organic polymer ferroelectric based on PVDF, which is safe and biocompatible. Such a photodetector [4], built on the basis of a hybrid quasi-autonomous FEP structure of the PVDF / P(VDF-TrFE) type in combination with MoS_2, already has more possibilities. The 2D MoS_2 ultrafine structure brings a great advantage for the heat dissipation of such a pyroelectric infrared detector. At the same time, the P(VDF-TrFE) polarization ferroelectric electric field significantly improves the photoconductive properties of MoS_2 and reduces the dark current and noise.

A further development of this approach is also work [5], which presents a version of the prototype photodetector with a broader spectral response, built on a quasi-autonomous hybrid structure of an organic FEP (P(VDF-TrFE)) and a two-dimensional semiconductor MoS_2. The two-dimensional 2D ultrafine structure of MoS_2 brings here a great heat dissipation advantage for such a pyroelectric infrared detector.

In addition, the electric field of ferroelectric polarization can not only restrain and reduce the dark current in the entire spectrum, but also change and narrow the band gap of MoS_2, thereby regulating the width of the optical absorption zone here, which significantly increases the photoconductive properties of MoS_2. The most impressive characteristic of this type of detector is that these mechanisms are synergistic [5].

In the present work, the main attention is focused to the study of the structural and physical properties, the interaction of FEP of the PVDF and P(VDF-TrFE) types with two-dimensional 2D structures of dichalcogenides of the MoS_2 type - using the methods of computer molecular modelling and calculations by different methods. These numerical and computer studies in this work are carried out on the basis of the developed and already well-tested approaches on other materials (PVDF, Graphene, Hydroxyapatite) using the density functional theory (DFT) [28-31] and quantum-chemical semi-empirical methods (such as PM3, ZINDO/1, etc.) [16-27, 49]. Theoretical studies and calculations of the properties of a number of TMD have already been carried out by various methods [32–36], and we use these results for comparison with data obtained in our calculations. In this work, we consider not only the TMD and FEP themselves, but also the models and properties of hybrid nanostructures based on them, for example, such as “PVDF + MoS_2” [31].

In the future, a similar simulation and study of nanomaterials and heterostructures for photodetectors based on $MoTe_2$ [37], $MoSe_2$ [38], $MoSe_2$-Cr [1, 39] and other dichalcogenides of transition metals and related ferroelectric nanostructures will be carried out.

2. COMPUTATIONAL METHODS AND DETAILS

The calculations were carried out using the first principles DFT methods, implemented in Vienna Ab Initio Simulation Package (VASP) [40–43]. The generalized gradient approximation (GGA) with the exchange-correlation potential was evaluated using the Perdew, Burke, and Ernzerhof (PBE) functional [43,44]. Core states were described by means of the projector augmented wave (PAW) method [45]. The values of the Kohn-Sham energies of the ground states of systems were calculated using plane waves with kinetic energy up to E_{cut} = 400 eV to expand the wave functions with fairly satisfactory convergence.

The primitive cell of single-layer MoS_2 containing one Mo atom and two S atoms was used under periodic boundary conditions. A vacuum space of 19 Å adopted along z-axis was used to be able to decouple possible periodic interactions. The valance electrons *s2p4* for S and *4p5s4d* for Mo were included in the PAW pseudopotentials.

For single layer MoS_2 calculation (with a direct band gap) GGA-PBE method was used taking into consideration of the van der Waals (vdW) interactions based on the method for VdW correction developed by Grimme S., Antony J., Ehrlich S., and Krieg S. [46] and named D3. This method is compatible with PBE and is implemented in VASP (as “PBE + D3”).

For the self-consistent calculations the Brillouin zone (BZ) was sampled by 11 x 11 x 1 Gamma-centred k-point grid obtained with Monkhorst-Pack scheme [47]. The band structure was evaluated on a path with k-spacing 0.05 $Å^{-1}$. The real-space grid of 20 x 20 x 128 points was chosen to keep approximately constant spacing proportional to the length of a_1, a_2, and a_3 lattice vectors. The experimental data [4, 35, 48] provides the lattice constants $a_1 = a_2 = a = b \sim 3.19$ Å of the known crystal structures MoS_2 and with $a_3 = c = \sim 19.0$ Å, which corresponds to the vacuum length between two adjacent layers in the supercell. The relevant grid density appears to be about ~ 6 points/Å along all the three directions.

To obtain the values of the energy, dipole moment, and polarization of the various MoS_2 and PVDF cluster structures the HyperChem package [49] was used with various quantum-mechanical semi-empirical methods. The method PM3 (Parametrization No. 3, developed by Stewart J.J.P. [50-52]) in the restricted Hartree-Fock (RHF) approximation was mainly used. This PM3 method is based on the AM1 method (Austin Model 1, developed by Dewar M.J.S., et al. [53]). However, in this our work another method named as ZINDO/1 [54] is used widely. This method ZINDO/1 is based on a modified version of the intermediate neglect of differential overlap (INDO) [55], which was developed by Michael Zerner [54] is most suitable for **transition metals**. An intermediate neglect of differential overlap (INDO, ZINDO/1 scheme retains some of the one-center terms of the overlapped integrals and the neglect of diatomic differential overlap (NDDO) [52] schemes used in these approaches keep all of the one-center terms. Zerner’s original INDO/1 used the Slater orbital exponents with a distance dependence for the first row transition metals only. However, in HyperChem [49] constant orbital exponents are used for all the available elements too, as recommended by Anderson, Edwards, and Zerner [54].

The main part of all quantum-chemical calculations in HyperChem was made using Single Point (SP) calculation method, which allow to obtain all necessary molecular electronic orbitals energy data values, such as, energy of the highest occupied molecular orbital (HOMO) and the lowest unoccupied molecular orbital (LUMO). Difference of these energies determine the forbidden band gap $E_g = E_{LUMO} - E_{HOMO}$. For some cases, when is necessary to taken into account the changes of geometry of the molecular systems, the optimization of molecular systems and finding of their optimal geometry is performed in this work using the Polak–Ribere (conjugate gradient method) algorithm, included in HyperChem package [49]. This approach is a especially important for the case of the dipole momentum rotation switching (and polarization switching) in the applied electric field at the critical point of the systems, such as, phase transition and reversal point of the hysteresis loop of the ferroelectric polar system. Simulation of the system under an imitated applied constant electric field is available in HyperChem packages too [49].

3. RESULTS AND DISCUSSION

Results of calculations performed using VASP [40-43] are shown on Fig. 1., where is presented the structure of the single monolayer MoS_2 with several unit cells (top and side views – Fig. 1 a, b). The lattice constant from self-consistent GGA-PBE calculations (a = 3.18999 Å ~ 3.19 Å) is close to the experimental data [33, 48] and theoretical value of other authors [32, 35, 56].

The electronic band structure obtained for single-layer MoS_2 with E_g = 1.632 eV, is presented on Fig. 1 c. It was intensively investigated recently by both experiments and theory [2-5, 32-39, 56]. The data obtained by different authors varies in some wide range.

A direct band gap, for example, of about 1.75 eV was obtained from the measurements [2]. The dispersion of bandgap in the range of 1.75 -1.90 eV in experiments may be come from the different preparation and measurement methods. Emilio Scalise [56] reported a value of 1.72 eV from GGA-PBE method calculation. The theoretical findings on direct bandgap calculations disperse also from 1.63 eV up to 2.76 eV. (depending on the exchange and correlation functionals used) [35]. Otherwise, C. Ataca [36] calculated a direct band gap of about 1.63 eV by GGA-PBE method taking into consideration of the van der Waals corrections (vdW) [46], and 1.87 eV by linear density approximation (LDA) method. As it can be seen, the LDA data turn out to be somewhat overestimated, while taking into account van der Waals interactions seems to give more realistic results. Data recently obtained by Wang et al. (published in Supplementary Materials section to [4]) shown very close similar data with E_g = 1.63 eV (Fig. 2 a).

It is worth to mention that the width of the band gap E_g significantly depends here on the applied

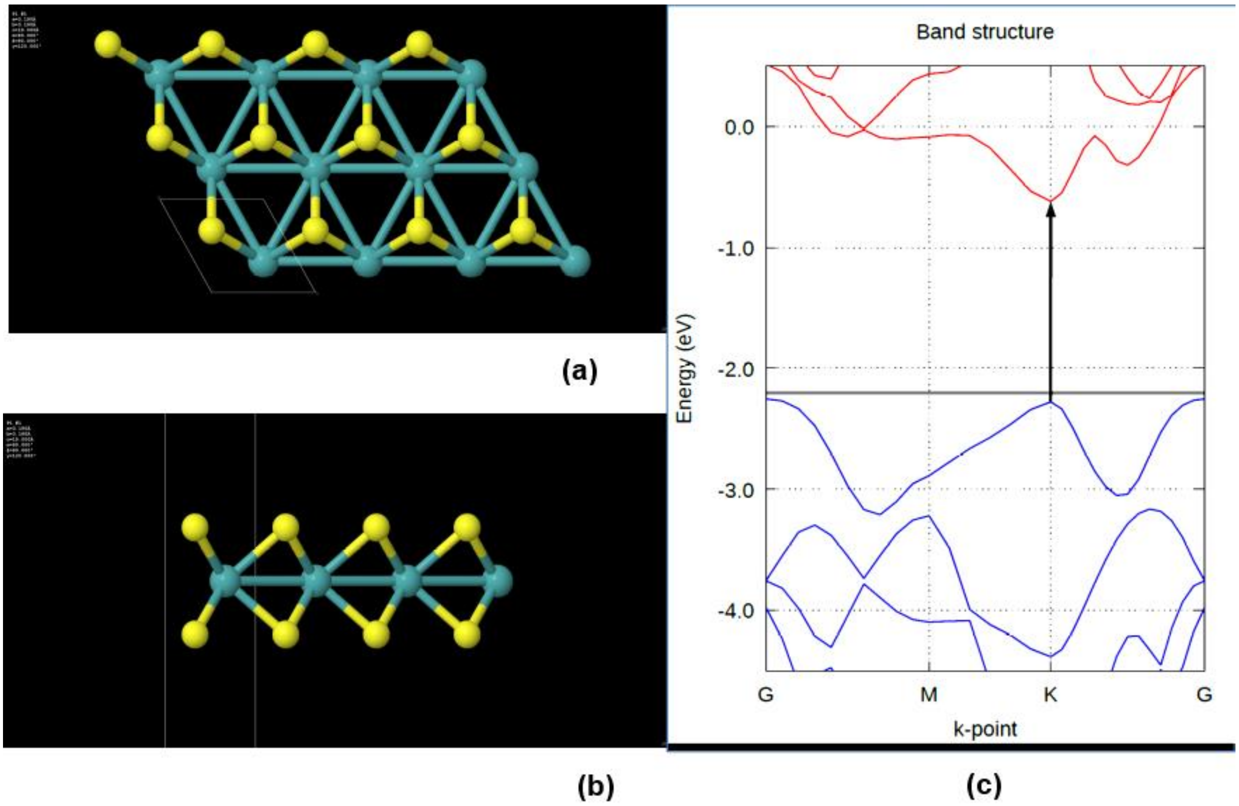

Figure 1. The structure of single-layer MoS_2 (obtained using Jmol after VASP calculations): a) top view, b) side view; and c) the computed electronic band structure of MoS_2 single monolayer with direct band gap transition along k-point variation with direct transition localization at K with computed energy value E_g = 1.632 eV.

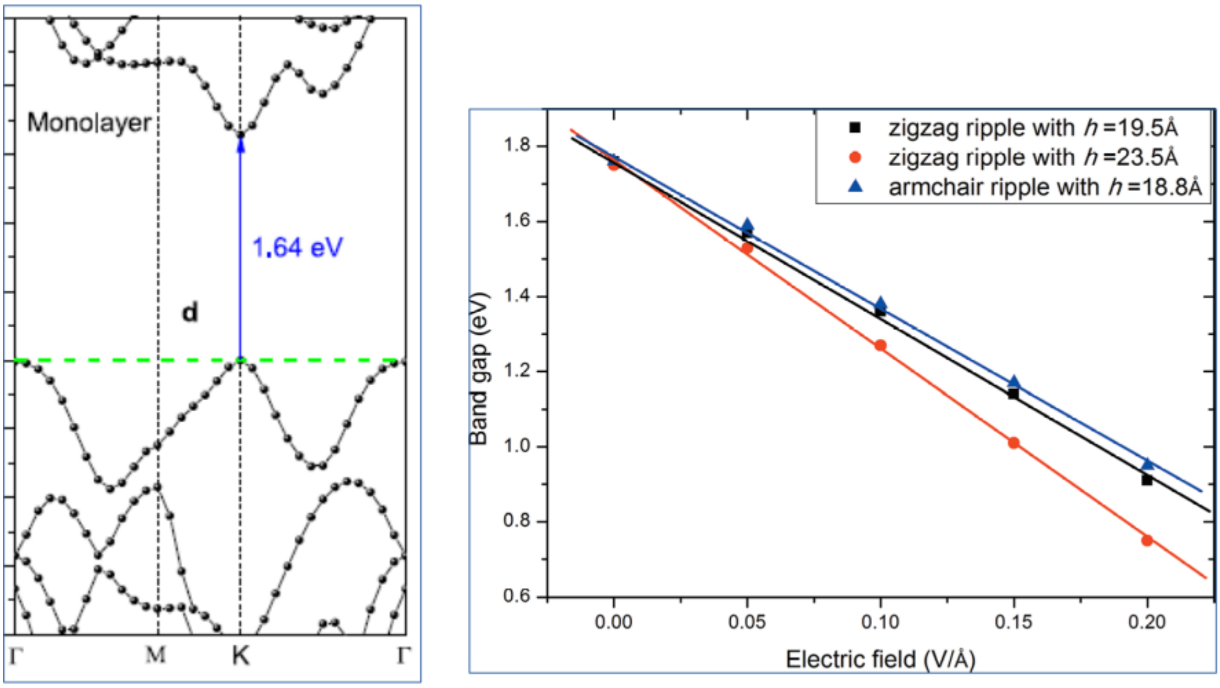

(a) (b)

Figure 2. The band gap computed by DFT method [4] (a) and dependence E_g (E) from [35] (b).

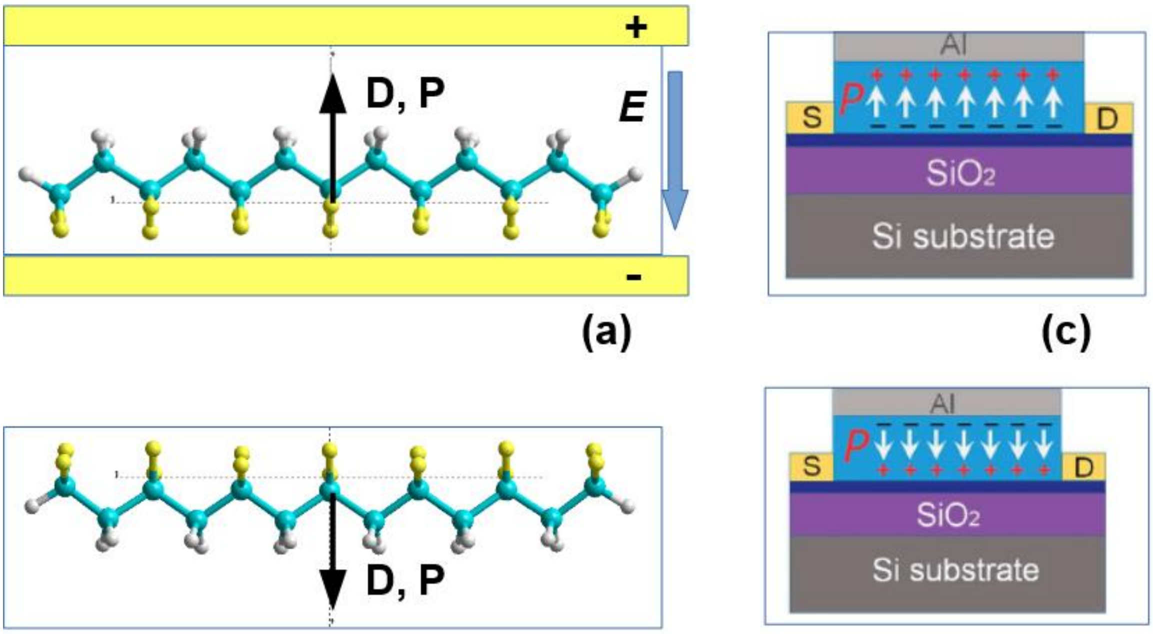

(a) (c)

(b) (d)

Figure 3. The PVDF single layer model structure under applied electric field E: a) direct position, b) switched on the opposite orientation position, c) and d) show the similar design of experimental units from Wang et al. work [4]. (D and P are the dipole moment and polarization of the PVDF chain of single layer, consequently).

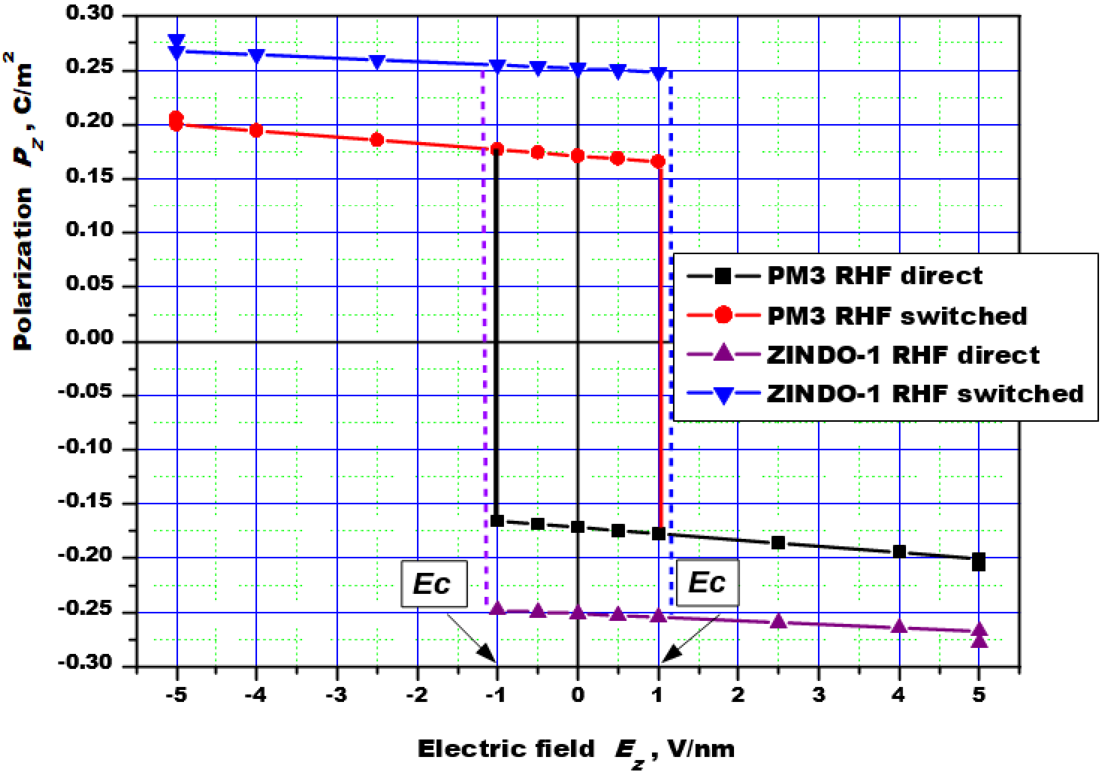

Figure 4. Hysteresis loop of the polarization depending on electric field P(E), computed by both PM3 and ZINDO/1 methods in RHF approximation using HyperChem package [49].

both experimentally and theoretically [2-5, 34-39]. Moreover, this dependence is different (as well as the value of E_g itself at an electric field $E = 0$) for different multi-layered MoS_2 structures (besides single mono- layer, were studied bilayer MoS_2 [32, 33], triple-layers MoS_2 [4]). But here we are primarily interested in the single MoS_2 structure with direct bandgap.

In particular, a similar structure was recently investigated and calculated in [35] and this dependence is shown in Fig 2 b. Typical values of the applied electric field E in the range of 0.0–0.001...0.2 V/Å = 0.0 — 0.01...2 V/nm lead to a change in E_g from 1.7 eV to 1.0 - 0.6 eV. The band gap E_g value as a function of electric field is displayed in Figure 2b for single MoS_2 layer structure (from work [35]). Despite the ripple character of studied MoS_2, it is clearly shown that E_g is linear dependent on electric field for any case. The similar linear relationship of E_g with rise of the electric field was reported also in the other transition-metal dichalcogenide, such as, bilayers under external electric field [33].

Among other things, it turned out that this range of variation of E_g ~ 1.8 - 0.6 eV is very important for optical measurements. From experimental studies and the bandgap calculations, it can be seen that the single-layer MoS_2 seems to be active for visible light absorption spectrum. For example, the peaks of the imaginary dielectric constant (which is sully used for measures the light absorption ability of materials) lie among the visible light range (350 nm – 700 nm, or 0.34 eV – 1.77 eV) for single-layer MoS_2. Since it would display high absorption of the sunlight and could be ideal for various photocatalysts applications, etc.

Another important point here was the search for the most suitable tools for controlling and regulating the change in the width of E_g in the MoS_2 layers of the vehicle, including, by influencing on MoS_2 samples by an electric field. The problem and the important task here was to find such a method

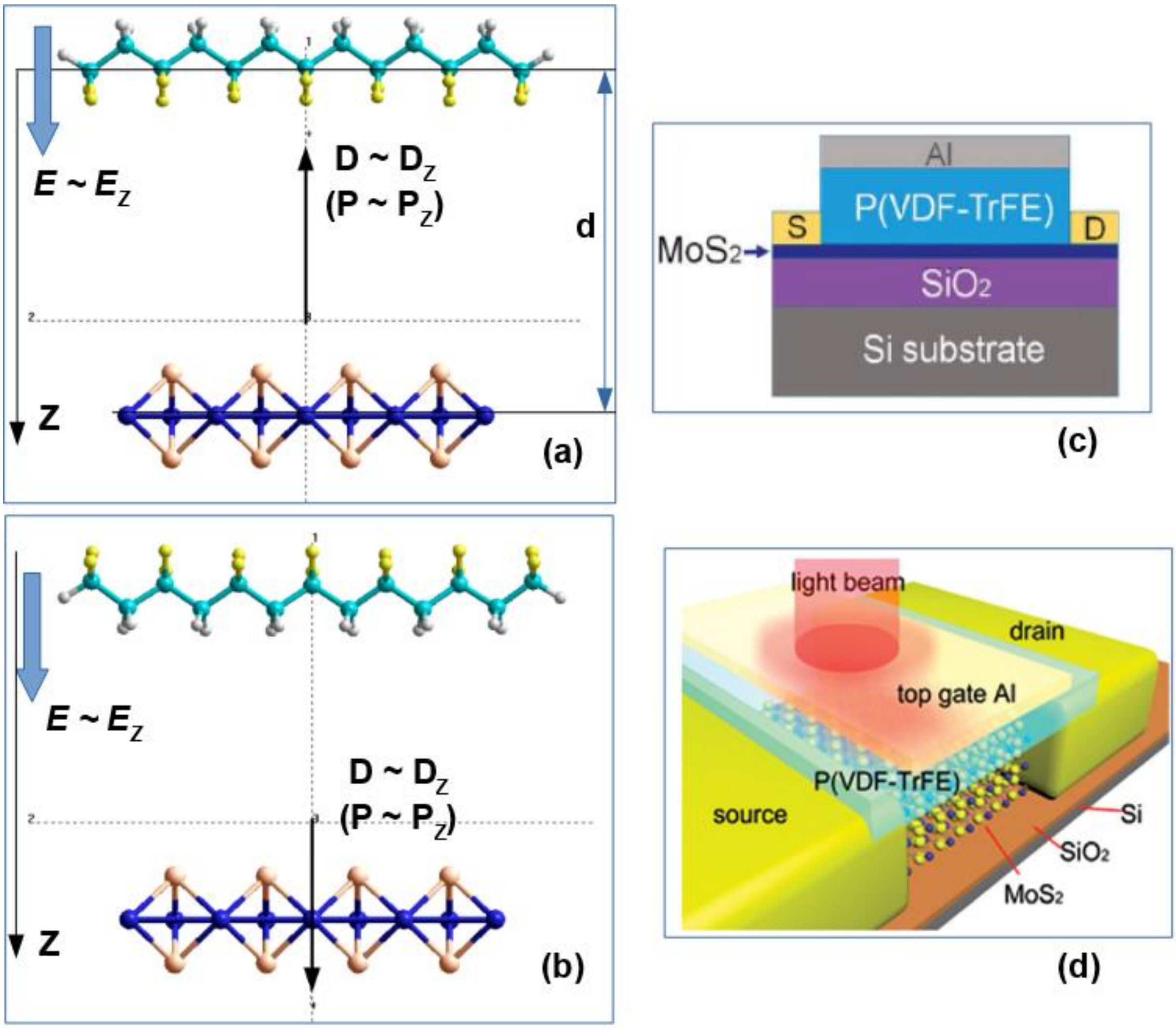

Figure 5. The MoS_2 single monolayer model interacting with PVDF layer (“PVDF + MoS_2” model): a) with direct PVDF orientation of the polarization vector P and with atoms F directed to atoms S, b) with switched PVDF on the opposite orientation of the polarization vector P and with atoms H directed to atoms S of MoS_2, c) and d) present the corresponding samples design of the hybrid structure configuration, which was used in Wang et al. work [4].

and means that would allow us the manipulation at the nanoscale, at sufficiently small micro-sizes, to create the appropriate technology, nano-devices and equipment.

It turned out that for this purpose, embedded layers of such a ferroelectric polymer films as PVDF and its copolymers P (PVDF-TrFE) can be very convenient. These materials are capable of creating and maintaining their spontaneous ferroelectric polarization just at the nanoscale sizes. And the electric field created by their polarization is capable of penetrating into the MoS_2 layers and affecting its E_g.

This idea was realized by Wang et al., for example, in their work [4].

It should be taken into account that the value of the PVDF polarization itself also depends on the electric field, which can be applied to layers of PVDF sandwiched between two electrodes. Thus, it is possible to easily change and render both the magnitude of this polarization and the width of the bandgap E_g in MoS_2 layers at the nano level.

The magnitude and direction of polarization P of this polymer ferroelectric is easily controlled by applying an electric field to the PVDF layers. It is also important here that on the basis of this polymer ferroelectric it is possible to create ultrathin layers up to one monolayer with a thickness of $d \sim 0.5$ nm, which nevertheless has a highly ordered polar structure. Practically important polymer

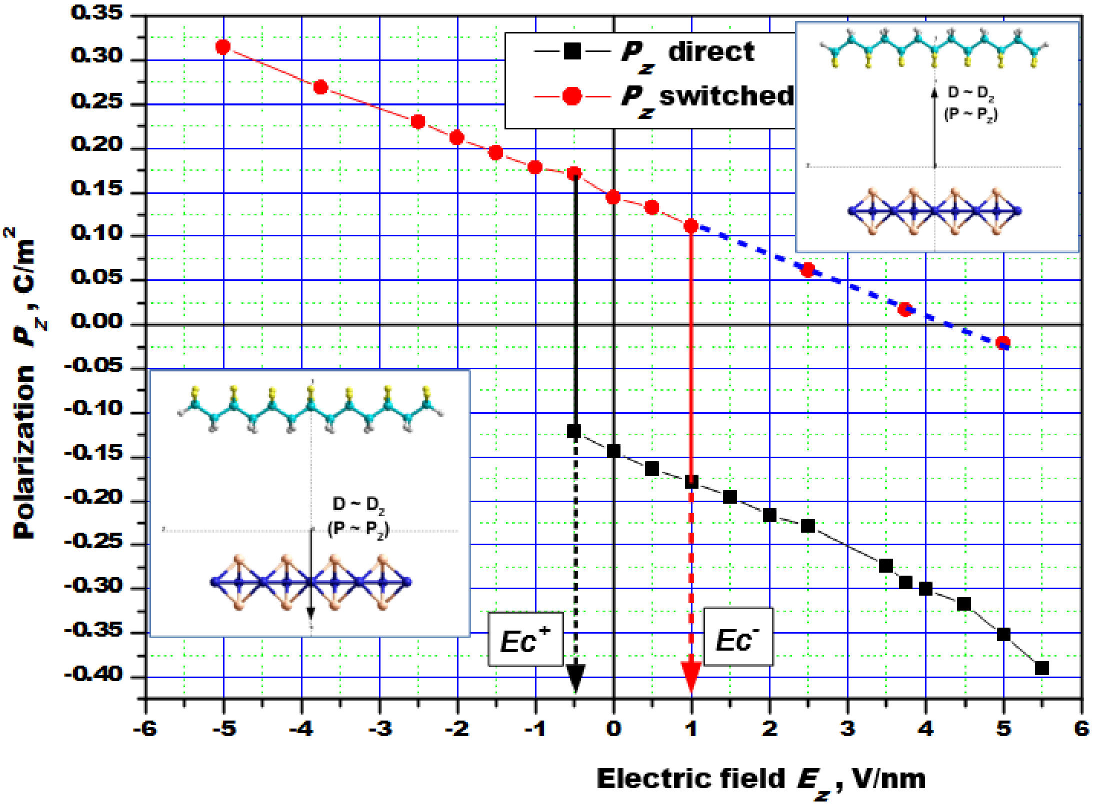

Figure 6. Computed dependence *P*(*E*) for the hybrid “MoS_2+PVDF” model with hysteresis loop behaviour, having the asymmetric *P*(*E*) branches and various coercive field E_c^+ and E_c^-.

structures of various thicknesses, including copolymers based on PVDF with tri-fluorine-ethylene (P (VDF-TrFE), can be easily removed either by ultracentrifugation methods (spun or spin coating films, with thickness ~ 100-300 nm) or by Langmuir-Blodgett (LB) technique (for ultra-thin films 0.5 - 100 nm). And these films are now quite well studied, including by the methods of molecular modeling [12-22].

In this work, we consider such a hybrid structure of «PVDF + MoS_2» - using the approaches of computer molecular modeling methods. First of all, we will consider and evaluate PVDF itself their main characteristic features and properties that allow them to be applied as a control factor on the E_g inside MoS_2 structure. This first model of the PVDF single layer and its behaviour in electric field *E* is shown in Fig. 3.

It is important that the polarization P and the field created by *P* outside the PVDF layers also depend on the electric field applied to the PVDF layers. Changing the magnitude and direction of the applied field *E* changes the magnitude of polarization *P* and switches the direction of polarization and, accordingly, changes the magnitude of the electric field induced in the MoS_2 layers.

We here simulate these properties, calculate and investigate the methods of semi-empirical calculations in the HyperChem software package. Here we have enough experience of such calculations [16-27]. The example of the main results and features for such simple PVDF chain (layer), computed by two semi-empirical quantum-chemical methods, is presented on Fig. 4. The main peculiarity of PVDF behaviour in applied electric field is following: 1) proportional rise of the polarization in the direct electric field, 2) switching on the opposite orientation of the polarization

Table 1. Computed data for both PM3 and ZINDO/1 methods at the distance d between two components of the "MoS_2+PVDF" model: d=10 Å, RHF approximation, both MoS_2 and PVDF, total calculating volume of the system V= 469.96 Å^3.

E_z, V/nm	D_z, Debye	$\|P_z\|$, C/m^2	$\|E_z^*\|=$ $=P_z/(2\varepsilon\varepsilon_0)$, V/nm	E HOMO, eV	E LUMO, eV	E_g, eV
ZINDO/1						
-1.0	-15.2632	0.1083	1.22	-6.235692	-1.790490	4.445202
-0.5	-19.0451	0.1352	1.53	-6.295287	-1.889087	4.406200
0.0	-20.4119	0.1449	1.64	-6.065749	-1.996101	4.069648
0.25	-21.7524	0.1544	1.74	-6.324941	-1.654380	4.670561
0.5	-21.9214	0.1556	1.76	-6.231306	-1.912776	4.328530
1.0	-25.7201	0.1825	2.06	- 6.305033	-1.865325	4.439708
2.5	-32.1791	0.2284	2.58	-6.09897	-1.981790	4.117167
4.0	-39.1240	0.2777	3.14	-5.116526	-1.968208	3.148328
5.0	-43.8091	0.3109	3.51	-4.040537	-2.051025	1.989512
PM3						
-1.0	-	-	-	-	-	-
-0.5	-13.4113	0.0952	1.075	-9.569354	-3.372284	6.197070
0.0	-14.3315	0.1017	1.15	-9.563627	-3.360310	6.203317
0.25	-14.8299	0.1053	1.19	-9.422036	-3.280216	6.141820
0.5	-15.2687	0.1084	1.22	-9.533896	-3.335629	6.198267
1.0	-16.0992	0.1143	1.29	-9.451263	-3.760474	5.690789
2.5	-19.0066	0.1349	1.59	-9.530275	-3.347384	6.182891
4.0	-21.8701	0.1547	1.75	-8.486326	-3.464778	5.021548
5.0	-23.6958	0.1677	1.89	-7.425726	-3.320158	4.105568

vector P under influence of the electric field E, when E reached its critical coercive values E_c.

The simplest model of the more complex hybrid structure, consisting of PVDF and MoS_2 single layer, is shown in Fig. 5. This model we also investigate by various methods from HyperChem package software [49]. Note that here besides PM3 here we wide use the ZINDO/1 method, available for transition metals. In any case we compare the data obtained by both methods for the case of the distance between PVDF and MoS_2 layer d = 10 Å (see below in Table 1).

The dependence $P(E)$ have hysteresis loop character with switching points at the $E = \pm E_c$ (Fig. 4).

For hybrid model "MoS_2 + PVDF" (Fig. 5) this behaviour have the similar character, but transforming to the more complex dependence with two asymmetric branches of the polarization P behaviour (up and down zero field E) and having two different coercive field E_c^+ and E_c^- (Fig. 6).

For comparison computed data of both used semi-empirical RHF methods (PM3 and ZINDO/1), the calculations performed at the distance d = 10 Å (between PVDF and MoS_2 components) were presented in the Table 1.

In HyperChem software after self-consistent calculations of the molecular structures by any quantum-chemical semi-empirical methods (as well by *ab initio* and DFT methods, included into HyperChem package) the data resulted and obtained have following main magnitudes (and its values in corresponding units): 1) dipole moment (in Debye unit), 2) total energy (in a. u. or can be converted to other units too), 3) energy of the highest occupied molecular orbital (HOMO in eV units) and energy of the lowest unoccupied molecular orbital (LUMO, eV), etc. We can

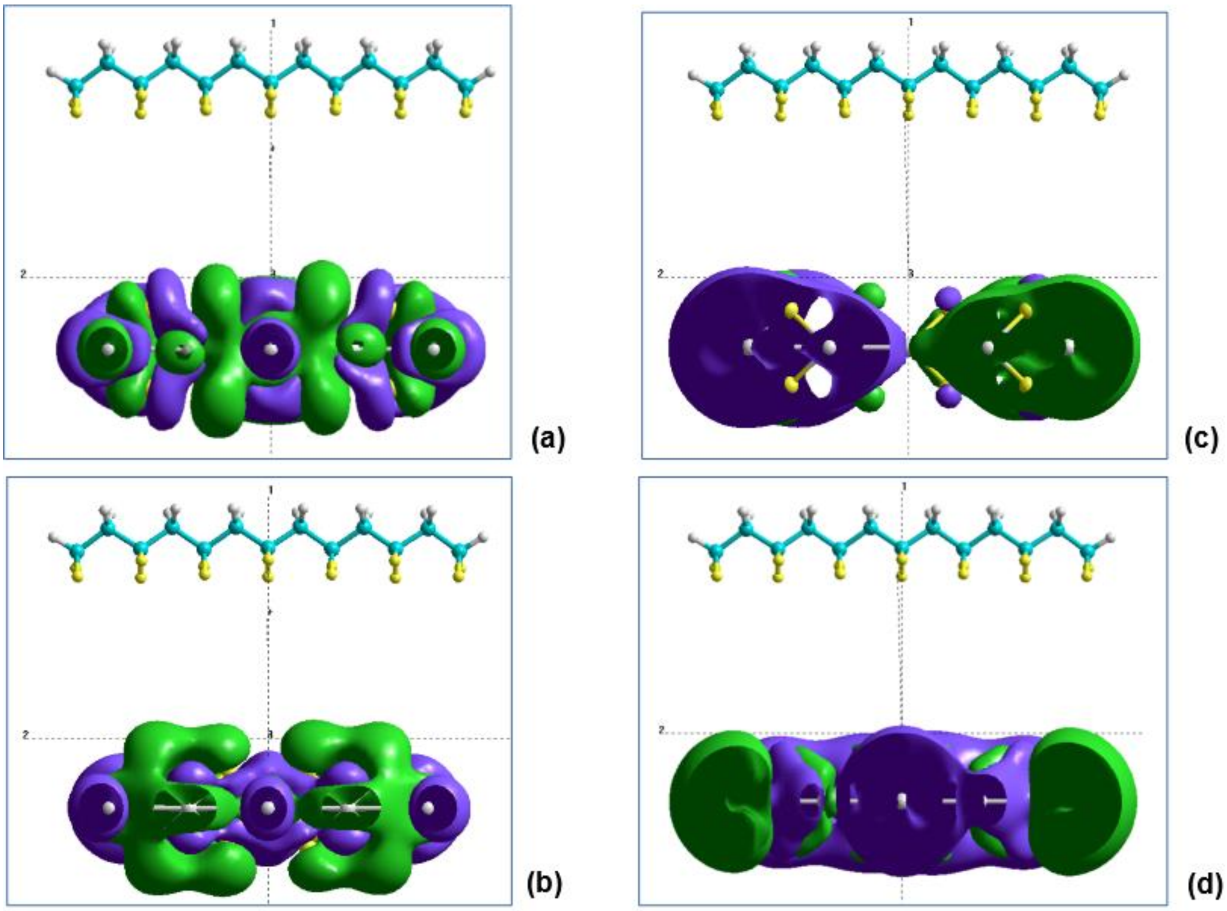

Figure 7. Electronic molecular orbitals for main energy states of the hybrid "MoS_2+PVDF" model and using the different semi-empirical computing methods:
a) LUMO and b) HOMO computed by PM3 in RHF approximation;
c) LUMO and d) HOMO computed by ZINDO/1 in RHF approximation.

calculate also the volume V, using special program. The band gap E_g = E LUMO – E HOMO. These data are presented in Table 1.

As usual, the value of the polarization P is obtained from dipole moment D (in Debye units):

$$P = 3.33558255*D/V \text{ (in } C/m^2\text{)},$$

where V is structure's volume on the Van der Waals surface.

Here we should note that, the prominent properties of this hybrid structure arise and benefit from the ferroelectric-polarization-induced ultra-high electric field of the PVDF (or P(VDF-TrFE) as in real usual samples).

To determine and estimate the magnitude of this local electric field E_z* at the interface between PVDF and MoS_2 layers, which is created inside the MoS_2 layer from PVDF polarization P, we use the expression $E_z^* = P_z/(2\varepsilon\varepsilon_0)$. Here e is the dielectric constant (permittivity) of the material (for MoS_2 it is ε = 4 – 6 [57, 58], e_0 is the vacuum constant (ε_0 = $8.85 \cdot 10^{-12}$ C/(V·m)). For our estimation in this our work, and presented in Table 1 as an example for the calculations at d = 10 Å (as well for other estimations), we use the middle value e = 5.

As results, we obtained data for E_z* ~ 1-2 V/nm for PM3 calculations and more high values Ez* ~ 1.2 – 3.5 V/nm for ZINDO/1 at the interface distance d = 10 Å (see in Table 1). These data are some higher than estimations in [4] about of 0.5 V/nm. But, in [4] was used the experimental data for polarization estimation as remnant polarization ~ 7 mC·cm^{-2} = 0.07 C/m^2 ~ 0.1 C/m^2, which is less from our estimation. But, we must mentioned, that we consider an ideal and simplified PVDF model, while the experimental value of remnant polarization for P(VDF-TrFE) is some less then

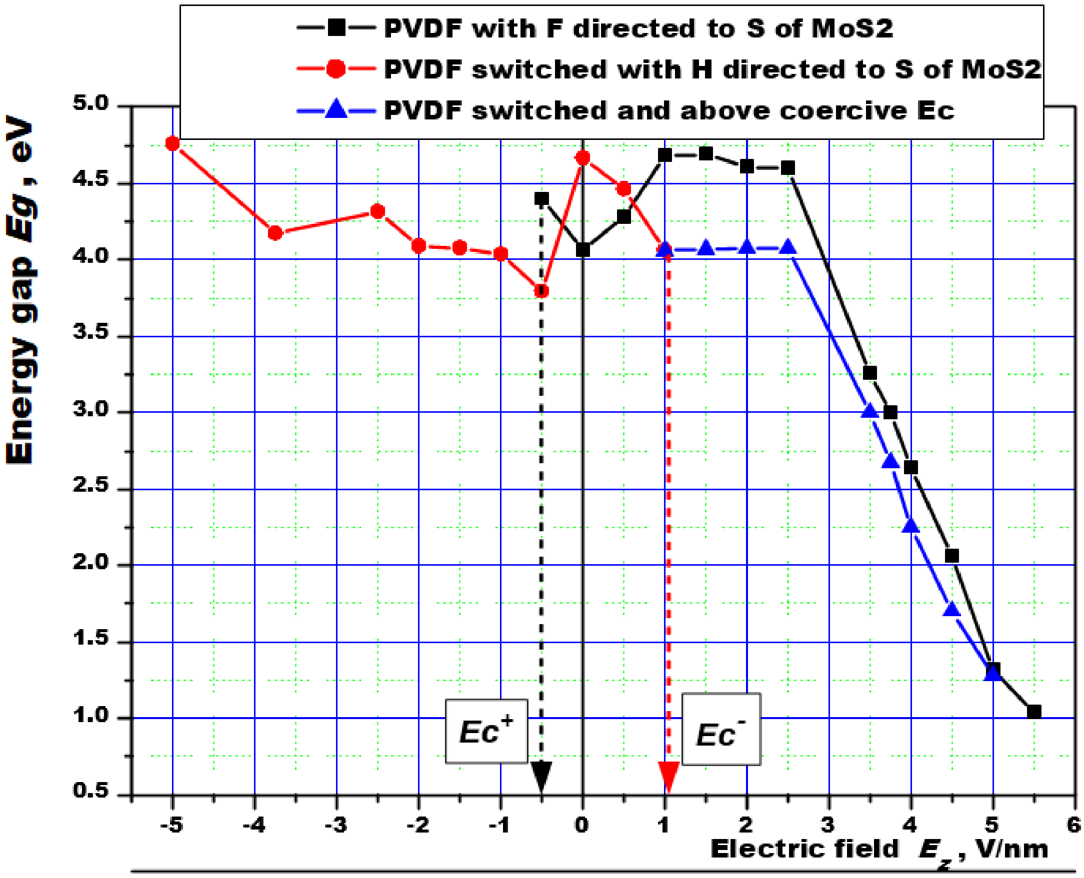

Figure 8. Computed energy band gap $E_g(E)$ for hybrid model “MoS_2 + PVDF” (Fig. 5 a) from the applied electric field *E*. This data is computed for distance d between MoS_2 and PVDF components d = 10 Å as one of example of this hybrid system.

computed one. Therefore, these estimates can be considered as quite close.

The more detailed computed data of the *P*(*E*) for this case are presented on the Fig. 6. These data shown two various branches of *P*(*E*) with different asymmetric coercive field. This asymmetry occurs because the MoS_2 layers is located only from one side of the PVDF layers (see on Fig. 5). As a result, we obtain the similar hysteresis behaviour of the *P*(*E*) for the hybrid model system (Fig 6) as for alone PVDF (Fig. 4), but it is shifted and having some different asymmetric shape of this hysteresis loop.

It means also that the additionally applied electric field *E* to the PVDF layers (using electrodes shown on Fig. 3) influences then trough risen polarization *P*(*E*) directly on the MoS_2 layer, which is positioned at the some distance *d* from PVDF place (Fig 5).

Further interesting and very important characteristic features is that the electronic molecular orbitals HOMO and LUMO are localized precisely on the MoS_2 layer positions remote at a distance d from the PVDF layer, as are shown in Fig. 7 (where are presented HOMO and LUMO computed using both PM3 and ZINDO/1 methods). Therefore, it is clearly show that the ferroelectric-polarization-induced ultra-high electric field of the PVDF (or P(VDF-TrFE) impact directly on the MoS_2 layer structure and influence on the E_g = E LUMO – E HOMO.

The next most important feature of this hybrid model system “PVDF + MoS_2” is that the dependence of band gap $E_g(E)$ clearly exists only

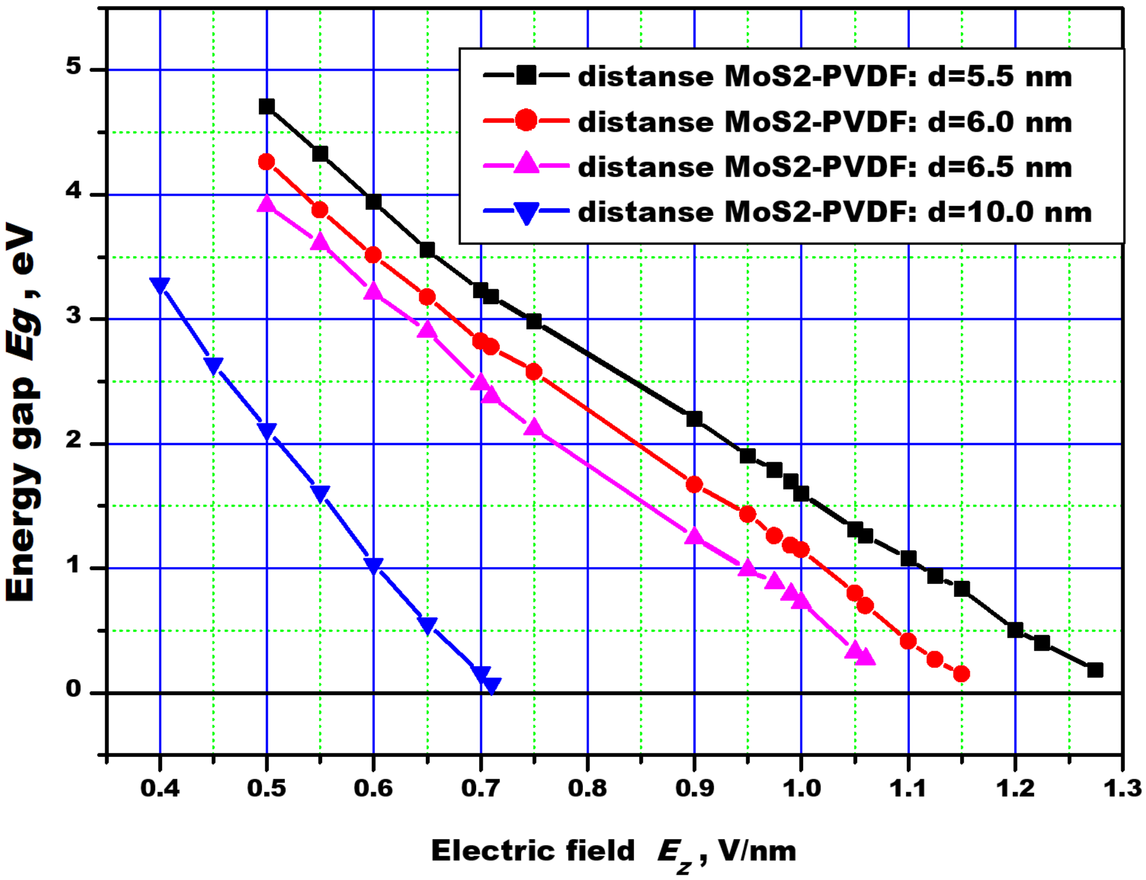

Figure 9. Computed dependence of the E_g (***E***) for different distances d - between MoS_2 and PVDF components of the hybrid model system.

for electric field E>0 (shown in Fig. 8), while for the *E*<0 we obtain only fluctuations around the average E_g value, close to the value existing without electric field. (see in Fig. 8 left side at the *E*<0).

The specific feature of the E_g (*E*) behaviour is again asymmetric dependence of the band gap E_g from electric field *E* and existence of two different coercive field E_c^+ and E_c^-, which limited the region of the existence of the electric field from PVDF layer impact on the MoS_2 layer.

The most characteristic feature here is that namely only at *E* > 0 there is a pronounced dependence of E_g from the electric field *E* (Fig. 8).

Another important founded and observed (possibly obvious) factor is the dependence on the distance between the PVDF and MoS_2 layers (Fig. 9). The calculations performed using ZINDO/1 method show that this dependence have the similar close to linear behaviour $E_g(E)$ (see details in Fig. 9) as it was founded for several different MoS_2 structures by various authors [4-6,32-35, 56].

The very important feature is that this behaviour depends also from the distance d - between MoS_2 and PVDF. it is characteristic that this behaviour $E_g(E)$ has a similar, close to linear type of behaviour at different distances d between both components of the hybrid structures. But at the same time, with an increase in this distance d, the slope of the dependence becomes steeper and it shifts along the *E* axis.

It is the results obtained here for very simple theoretical molecular models and they describe approximative results of its features and behaviours. But these data obtained show the main principal features of the E_g behaviour from electric field *E* and intermediate distance d between both nanostructures MoS_2 and PVDF, which would be very important for further practical design of the devise unit of the created photodetector samples.

The results obtained are, of course, somewhat different from the most precise DFT calculations.

But they are qualitatively very similar and reflect the main characteristics and dependencies. A more in-depth study will be carried out in further investigations using the DFT VASP methods.

4. CONCLUSION

Performed modelling and calculations presented in this study directly show that the band gap E_g of the MoS_2 layer is strongly affected by external electric field. The E_g changes are influenced, controlled and regulated by the electric field formed by a polarization in the ferroelectric polymer layers such as PVDF and its copolymers P(VDF-TrFE) depending on the discussed distance *d*. The electric field formed in the ferroelectric layers strongly affects the band gap E_g of the MoS_2 layered structure. The nano-size devices created on the basis of such hybrid nano-structures can be considered as the prototypes of the photodetectors and other photosensitive units for numerous practical applications. Further studies based on the most powerful DFT software (such as VASP, etc.) will open many new features for fundamental knowledges and practical usage.

ACKNOWLEDGEMENTS

The authors are greatly thankful to the Russian Foundation for Basic Researches (RFBR): grants # 19-01-00519_A and # 20-51- 53014_ A. The authors are indebted to the Phys. Dept. of the University of Aveiro (UA), Portugal, for the opportunity of using Linux-cluster for the computational studies within the framework of non-profit Scientific Agreement between UA and IMPB/KIAM.

Prof. Xiang-Jian Meng expresses his gratitude to the National Natural Science Foundation of China (NNSFC) for grant # 61574151 and Prof. Hong Shen – for grant # 62011530043.

REFERENCES

[1] A. Eftekhari. Tungsten dichalcogenides (WS_2, WSe_2, and WTe_2): materials chemistry and applications. *Journal of Materials Chemistry A*, **5** (35), 18299–18325 (2017).

[2] A. Splendiani, L. Sun, Y. Zhang, T. Li, J. Kim, C. Y. Chim, G. Galli, F. Wang. Emerging Photoluminescence in Monolayer MoS_2. *Nano Letters*, **10** (4), 1271–1275 (2010).

[3] O. Lopez-Sanchez, D. Lembke, M. Kayci, A. Radenovic, A. Kis. Ultrasensitive photodetectors based on monolayer MoS_2. *Nature Nanotechnology*, **8** (7), 497–501 (2013).

[4] Xudong Wang, Peng Wang, Jianlu Wang, Weida Hu, Xiaohao Zhou, Nan Guo, Hai Huang , Shuo Sun, Hong Shen, Tie Lin, Minghua Tang, Lei Liao, Anquan Jiang, Jinglan Sun, Xiangjian Meng, Xiaoshuang Chen, Wei Lu, and Junhao Chu. Ultrasensitive and Broadband MoS_2 Photodetector Driven by Ferroelectrics. *Adv. Mater.*, **27**, 6575–6581 (2015).

[5] Xudong Wang, Hong Shen, Yan Chen, Guangjian Wu, Peng Wang, Hui Xia, Tie Lin, Peng Zhou, Weida Hu,* Xiangjian Meng, Junhao Chu, and Jianlu Wang. Multimechanism Synergistic Photodetectors with Ultrabroad Spectrum Response from 375 nm to 10 µm. *Adv. Sci.*, **6(15)**, 1901050 (2019).

[6] A. K. Geim. Graphene: Status and Prospects. *Science.*, **324**, 1530–1534 (2009).

[7] X. Li, L. Tao, Z. Chen, H. Fang, et. al. Graphene and related two-dimensional materials: Structure-property relationships for electronics and optoelectronics. *Appl. Phys. Rev.*, **4**, 021306 (2017).

[8] A. K. Geim, I. V. Grigorieva. Van der waals heterostructures. *Nature*, **499**, 419–425 (2013).

[9] M. E. Lines, A. M. Glass. Principles and Applications of Ferroelectrics and Related Materials. Oxford: Clarendon (1977).

[10] T. T. Wang, J. M. Herbert, A. M. Glass. The Applications of Ferroelectric Polymers. New York: Chapman and Hall (1988).

[11] H. S. Nalwa. Ferroelectric Polymers. New York: Marcel Dekker (1995).

[12] A.V. Bune, Ch. Zhu, S. Ducharme, L. M. Blinov, V. M. Fridkin, S. P. Palto, N. G. Petukhova, S. G. Yudin. Piezoelectric and pyroelectric properties of ferroelectric Langmuir-Blodgett polymer films. *J. Appl. Phys.*, **85**, 7869 (1999).

[13] A. V. Bune, V. M. Fridkin, S. Ducharme, L. M. Blinov, S. P. Palto, A. V. Sorokin, S. G. Yudin, A. Zlatkin. Two-dimensional ferroelectric films. *Nature (London)*, **391**, 874-877 (1998).

[14] L.M. Blinov, V.M. Fridkin, S.P. Palto, A.V. Bune, P.A. Dowben, S. Ducharme, Two-dimensional ferroelectrics, *Physics-Uspekhi* **43**, 243–257 (2000).

[15] V. Fridkin, S. Ducharme. Ferroelectricity at the Nanoscale. Basics and Applications. Berlin: Springer-Verlag (2014).

[16] V. S. Bystrov and V. M. Fridkin. Domain and homogeneous switching in ferroelectrics. On the 75th anniversary of the Landau–Ginzburg theory of ferroelectricity. *Ferroelectrics*, (2020).

[17] V. S. Bystrov, V. M. Fridkin. Two-dimensional ferroelectrics and homogeneous switching. To the 75th anniversary of the Landau—Ginzburg theory of ferroelectricity. *Phys. Usp.*, **63**, 417–439 (2020).

[18] E. Paramonova, V. Bystrov, Xiangjian Meng, Hong Shen, Jianlu Wang, V. Fridkin. Polarization switching in 2D nanoscale ferroelectrics: Computer simulation and experimental data analysis. *Nanomaterials*, **10** (9), 1841 (2020).

[19] V. S. Bystrov, E. V. Paramonova, I. K. Bikin, A. V. Bystrova, R. C. Pullar, A. L. Kholkin. Molecular modeling of the piezoelectric effect in the ferroelectric polymer poly(vinylidene fluoride) (PVDF). *J. Mol. Model.*, **19**, 3591–3602 (2013).

[20] V. S. Bystrov. Molecular modeling and molecular dynamic simulation of the polarization switching phenomena in the ferroelectric polymers PVDF at the nanoscale. *Physica B: Condensed Matter*, **432**, 21-25 (2014).

[21] E.V. Paramonova, S.V. Filippov, V.E.Gevorkya, L.A. Avakyan, X.J.Meng, B.B. Tian, J.L. Wang and V.S. Bystrov. Polarization switching in ultrathin polyvinylidene fluoride homopolymer ferroelectric films. *Ferroelectrics, 509, 143–157, (2017).*

[22] V. S. Bystrov, E. V. Paramonova, A. V. Bystrova, V. E. Gevorkyan, X. J. Meng, B. B. Tian, J. L. Wang, L. A. Avakyan. Analysis of the computational and experimental studies of the polarization switching in the PVDF and P(VDF-TrFE) ferroelectric films at the nanoscale. *Mathematical Biology and Bioinformatics*, **10** (2), 372-386 (2015).

[23] V. S. Bystrov, I. K. Bdikin, M. V. Silibin, D. V. Karpinsky, S. A. Kopyl, G. Goncalves, A. V. Sapronova, T. Kuznetsova, V. V. Bystrova. Graphene/Graphene oxide and polyvinylidene fluoride polymer ferroelectric composites for multifunctional applications. *Ferroelectrics*, **509**, 124–142, (2017).

[24] M. V. Silibin, V. S. Bystrov, D. V. Karpinsky, N. Nasani, G. Goncalves, I. M. Gavrilin, A. V. Solnyshkin, P. A. A. P. Marques, B. Singh, I. Bdikin. Local mechanical and electromechanical properties of the P(VDF-TrFE)-graphene oxide thin films. *Applied Surface Science*, **421**, Part A, 42-51 (2017).

[25] V. S. Bystrov, I. K. Bdikin, M. Silibin, D. Karpinsky, S. Kopyl, E. V. Paramonova, G. Goncalves. Molecular modeliбng of the piezoelectric properties in the Graphene/Graphene oxide and polyvinylidene fluoride (PVDF) polymer ferroelectric composites. *J. Mol. Mod.*, **23**, 128 (14 pages) (2017).

[26] V. S. Bystrov, M. V. Silibin, X. J. Meng, T. Lin, H. Shen, B. Tian, J. L. Wang, D. V. Karpynsky, A. V. Bystrova, E. V. Paramonova. Modelling of the Piezoelectric and Pyroelectric properties of the Ferroelectric composites thin films based on the polyvinylidene fluoride (PVDF) with Graphene and Graphene Oxide layers and fibers. *Nanomaterials Science & Engineering*, **2** (2), 83-92 (2020).

[27] V. S. Bystrov, I. K. Bdikin, M. V. Silibin, X. J. Meng, T. Lin, J. L. Wang, D. V. Karpynsky, A. V. Bystrova, E. V. Paramonova. Pyroelectric properties of the ferroelectric composites based on the polyvinylidene fluoride (PVDF) with graphene and graphene oxide. *Ferroelectrics*, **541**, 17–24 (2019).

[28] L. A. Avakyan, E. V. Paramonova, J. Coutinho, S. Öberg, V. S. Bystrov, L. A. Bugaev. Optoelectronics and defect levels in hydroxyapatite by first-principles. *J. Chem. Phys.*, **148**, 154706 (12 pages), (2018).

[29] V. S. Bystrov, L. A. Avakyan, E. V. Paramonova, J. Coutinho. Sub-Band Gap Absorption Mechanisms Involving Oxygen Vacancies in Hydroxyapatite. *J. Chem. Phys. C.*, **123** (8), 4856–4865 (2019).

[30] V. S. Bystrov, J. Coutinho, L. A. Avakyan, A. V. Bystrova and E. V. Paramonova. Piezoelectric, ferroelectric, and optoelectronic phenomena in hydroxyapatite with various defect levels. *Ferroelectrics*, Vol. **559** (1), pp. 45-55 (2020).

[31] V. S. Bystrov, H. Shen, X. J. Meng. Modeling of dichalcohgenide MoS_2 monolayers and its composites with PVDF/P(VDF-TrFE). In: 2nd International Conference on Nanomaterials Science and Mechanical Engineering. Book of Abstracts. (University of Aveiro, Portugal, July 9-12, 2019). Editors: I. Bdikin, B.Singh, R. Simoes. Publisher: UA Editora, Universidade de Aveiro (2019). - pages 163-164. ISBN 978-9732-789-544-1

[32] A. Ramasubramaniam, D. Naveh and E. Towe. Tunable band gaps in bilayer transition-metal dichalcogenides. *Phys. Rev. B*, **84**, 205325 (2011).

[33] N. Zibouche, P. Philipsen, A. Kuc and T. Heine. Transition-metal dichalcogenide bilayers: Switching materials for spintronic and valleytronic applications. *Phys. Rev. B*, **90**, 125440 (2014).

[34] T. Wozniak, P. Scharoch and M.J. Winiarski. Structural Parameters and Electronic Structure of Monolayers of Transition Metal Dichalcogenides from *Ab Initio* Calculations. *ACTA PHYSICA POLONICA A*, **129** (1A), A56-A58 (2016).

[35] Yunguo Li, Yan-Ling Li, C.M. Araujo, W. Luo and R. Ahuja. Single-layer MoS_2 as an efficient photocatalyst. *Catal. Sci. Technol.*, **3**, 2214 (2013).

[36] C. Ataca and S. Ciraci. Dissociation of H2O at the vacancies of single-layer MoS_2. *Phys. Rev. B*, **85**, 195410 (2012).

[37] Guangjian Wu, Xudong Wang, Yan Chen, Shuaiqin Wu, Binmin Wu, Yiyang Jiang, Hong Shen, Tie Lin, Qi Liu, Xinran Wang, Peng Zhou, Shantao Zhang, Weida Hu, Xiangjian Meng, Junhao Chu, and Jianlu Wang. $MoTe_2$ p–n Homojunctions Defined by Ferroelectric Polarization. *Adv. Mater.*, 1907937 (2020).

[38] Dan Li, Xudong Wang , Yan Chen, Sixin Zhu, Fan Gong, Guangjian Wu, Caimin Meng, Lan Liu, Lin Wang, Tie Lin, Shuo Sun,Hong Shen, Xingjun Wang, Weida Hu , Jianlu Wang, Jinglan Sun,Xiangjian Meng and Junhao Chu. The ambipolar evolution of a high-performance WSe_2 transistor assisted by a ferroelectric polymer. *Nanotechnology*, **29**, 105202 (2018).

[39] Yan Chen, Chong Yin, Xudong Wang, Yiyang Jiang, Haoliang Wang, Binmin Wu, Hong Shen, Tie Lin, Weida Hu, Xiangjian Meng, Piyi Du, Junhao Chu, Zongrong Wang,and Jianlu Wang, Multimode Signal Processor Unit Based on the Ambipolar WSe_2−Cr Schottky Junction. *ACS Applied Materials & Interfaces*, **11**(42), 38895-38901 (2019).

[40] VASP (Vienna Ab initio Simulation Package). Available online: https://www.vasp.at/ (accessed on 17 November 2020).

[41] G. Kresse, J. Furthmuller. Ecient iterative schemes for ab initio total-energy calculations using a plane-

wave basis set. *Phys. Rev. B Condens. Matter Mater. Phys.*, **54**, 11169–11186 (1996).

[42] G. Kresse, D. Joubert. From ultrasoft pseudopotentials to the projector augmented-wave method. *Phys. Rev. B Condens. Matter Mater. Phys.*, **59**, 1758–1775 (1999).

[43] J. P. Perdew, K. Burke, M. Ernzerhof. Generalized Gradient Approximation Made Simple. *Phys. Rev. Lett.*, **77**, 3865–3868 (1996).

[44] J. Paier, R. Hirschl, M. Marsman, G. Kresse. The Perdew-Burke-Ernzerhof exchange-correlation functional applied to the G2-1 test set using a plane-wave basis set. *J. Chem. Phys.* **122**, 234102 (2005).

[45] P. E. Blochl. Projector augmented-wave method. *Phys. Rev. B Condens. Matter Mater. Phys.*, **50**, 17953–17979 (1994).

[46] S. Grimme, J. Antony, S. Ehrlich, S. Krieg. A consistent and accurate ab initio parametrization of density functional dispersion correction (dft-d) for the 94 elements H-Pu. *J. Chem. Phys.*, **132**, 154104 (2010).

[47] H. J. Monkhorst, J. D. Pack. Special points for Brillouin-zone integrations. *Phys. Rev.*, **13**, 5188–5192 (1976).

[48] D. Yang, S. Jiménez Sandoval, W. M. R. Divigalpitiya, J. C. Irwin, and R. F. Frindt. Structure of single-molecular-layer MoS_2. *Phys. Rev. B*, **43**, 12053 (1991).

[49] Hypercube Inc. HyperChem, versions 7.51 and 8.0; Hypercube Inc.: Gainesville, FL, USA, 2002. Available online: http://www.hyper.com/?tabid=360 (accessed on 7 November 2020).

[50] J. J. P. Stewart. Optimization of Parameters for Semiempirical Methods. I. Method. *J. Comput. Chem.*, **10**(2), 209–220 (1989).

[51] J. J. P. Stewart. Optimization of parameters for semiempirical methods. II. Applications. *J. Comput. Chem.*, **10**(2), 221–264 (1989).

[52] J. J. P. Stewart. Optimization of parameters for semiempirical methods V: modification of NDDO approximations and application to 70 elements. *J. Mol. Mod.*, **13**(12), 1173–1213 (2007).

[53] M. J. S. Dewar, E. G. Zoebisch, E. F. Healy, J. J. P. Stewart. Development and use of quantum-mechanical molecular models. 76. AM1: A new general purpose quantum mechanical molecular model. *J. Am. Chem. Soc.*, **107**, 3902–3909 (1985).

[54] W. P. Anderson, W. D. Edwards, M. C. Zerner. Calculated spectra of hydrated ions of the first transition-metal series. *Inorg. Chem.*, **25**, 2728–2732 (1986).

[55] L. A. Carreira, W. B. Person. INDO (intermediate neglect of differential overlap) calculations of properties of molecular complexes. *J. Am. Chem. Soc.*, **94**(5), 1485-1495 (1972).

[56] E. Scalise, M. Houssa, G. Pourtois, V. Afanas’ev, A. Stesmans. Strain-Induced Semiconductor to Metal Transition in the Two-Dimensional Honeycomb Structure of MoS_2. *Nano Res.* **5** (1), 43-48 (2012).

[57] X. Chen, Z. Wu, S. Xu, et al. Probing the electron states and metal-insulator transition mechanisms in molybdenum disulphide vertical heterostructures. *Nat. Commun.*, **6**, 6088 (2015).

[58] E. J. G. Santas, E. Kaxiras. Electrically Driven Tuning of the Dielectric Constant in MoS_2 Layers. *ACS Nano*, 7 (12), 10741-10746 (2013).